

Benchmarking and modeling of analog and digital SRAM in-memory computing architectures

Pouya Houshmand
MICAS, KU Leuven
Leuven, Belgium
pouya.houshmand@kuleuven.be

Jiacong Sun
MICAS, KU Leuven
Leuven, Belgium
jiacong.sun@kuleuven.be

Marian Verhelst
MICAS, KU Leuven
Leuven, Belgium
marian.verhelst@kuleuven.be

Abstract—In-memory-computing is emerging as an efficient hardware paradigm for deep neural network accelerators at the edge, enabling to break the memory wall and exploit massive computational parallelism. Two design models have surged: analog in-memory-computing (AIMC) and digital in-memory-computing (DIMC), offering a different design space in terms of accuracy, efficiency and dataflow flexibility. This paper targets the fair comparison and benchmarking of both approaches to guide future designs, through a.) an overview of published architectures; b.) an analytical cost model for energy and throughput; c.) scheduling of workloads on a variety of modeled IMC architectures for end-to-end network efficiency analysis, offering valuable workload-hardware co-design insights.

Index Terms—Machine learning processing, DNN acceleration, mixed-signal computing, analog in-memory computing, digital in-memory computing

I. INTRODUCTION

The need for executing AI workloads on edge devices, characterized by limited power budgets and area constraints, results in large research interest in custom hardware accelerator design, with large advancements in a short time frame [1]. As these workloads require a significant amount of data movement between the processor and the memory, traditional Von Neumann architectures have proven unsuitable for the application [2]. To handle this data transfer bottleneck, a functional approach adopted from the early published designs is to parallelize the computing units in space, thus allowing for a higher degree of spatial multi-cast reuse of the operands as they are fetched from memory. Conventional accelerators [3] thus are composed of a 2D array of processing elements (PE), each of which contains a multiply-accumulate (MAC) unit (or vector) and small register files to store operands. These operands are fetched from larger memories outside the PE array and distributed in space across the processing elements, according to the spatial parallelization scheme adopted for the workload (also called "spatial unrolling") [4]. Yet, memory interfacing remains a performance-limiting aspect of modern neural accelerators. In recent years, in-memory computing (IMC) has therefore emerged as a promising alternative to PE-based accelerators, by performing the MAC operations near/in the memory cells directly. This allows to greatly reduce access overheads and enables massive parallelization opportunities, with potential orders of magnitude improve-

ments in energy efficiency and throughput [5]. Most recent IMC designs published in the literature are focused on analog IMC (AIMC), where the computation is carried out in the analog domain. While this approach ensures extreme energy efficiencies and massive parallelization, the analog nature of the computation and the presence of intrinsic circuit noise and mismatches compromises the output accuracy. Furthermore, the rigid structure of the computation's dataflow limits the spatial mapping possibilities. To avoid the hurdles of AIMC, digital in memory computing (DIMC) is lately gaining more interest as a valid alternative, thanks to its noise-free computation and more flexible spatial mapping possibilities, trading off added flexibility and accurate computation for less energy efficiency. These new opportunities stemming from AIMC and DIMC resulted in many recent implementations and publications in the literature. However, these works vary strongly in terms of hardware architecture, array dimensions, and silicon technology. This makes it difficult to grasp their relative strengths, trends and future directions. While several works assess and discuss IMC trends qualitatively [5]–[12], only few aim at quantitatively modeling or benchmarking architectural strategies. The latter, moreover, primarily focus on AIMC designs [5], [13]–[19], while there is a lack of DIMC modeling efforts. Similarly, for mapping space explorations, most of the focus has been dedicated to AIMC designs, while lacking DIMC assessment [16], [17], [20], [21].

To this purpose, this paper aims at:

- Providing a comprehensive assessment of recently published AIMC and DIMC chips, in order to understand through benchmarking the capabilities and limitations of the two design paradigms.
- Provide a unified analytical model for IMC architectures, validated against numerous design points from literature.
- Integrate the model into ZigZag [4], a design space exploration (DSE) framework for hardware accelerators. This allows to compare different AIMC / DIMC hardware design points, data flows and mappings in terms of energy and throughput efficiency, towards insights on optimal design points for targeted tinyMLperf workloads [22].

To quantitatively compare the IMC designs reported in literature, we collect those works that target MVM operations and non binary neural networks (BNNs). The BNN restriction is due to the fact that 1) for AIMC the A/D conversion is substituted with an energy efficient sense-amplifier (at the cost of added quantization noise), skewing the efficiencies comparison and 2) the tinyMLPerf benchmark [22] does not include BNN models. Only IMC works that report their performance with 50% sparsity are retained to guarantee fairness in the comparison. This results in following selected AIMC designs: [24], [26]–[39]; and DIMC designs: [40]–[42]. For each implementation, Figure 4 plots the derived energy efficiency (TOP/s/W) and computational density (TOP/s/mm²) from the papers’ reported peak efficiencies. Dashed, resp. solid lines connect different results stemming from the same chip for across different operand precision, resp. supply voltages. Other works ([6], [43]) benchmark different designs on bit-normalized metrics (e.g. 1-b TOPs/W, 1-b TOP/s); this work does not employ such metrics as they would provide a distorted representation of the design landscape. The impact of operand precision will become more clear in the modeling Sec. IV.

Fig. 4, reveals that [26] achieves the best peak energy efficiency of ~ 1800 TOP/s/W among AIMC designs. This is possible through the optimized design of ADCs and DACs and a large array that amortizes their costs – making the array power consumption the dominant contribution instead of the ADCs. The best computational density is achieved by [32], a design implemented in 7nm with Flash ADCs, as opposed to the commonly used SAR-ADCs; this design choice in turn affects the energy efficiencies, which are not optimal. Multi-core architectures have also emerged recently to reduce the lack of flexibility in AIMC dataflows by either unrolling the OX dimension across macros [29] or using smaller arrays [30]–[32], [34], with benefits both in terms of utilization and signal margin on the ADCs. It is to be noted that in AIMC designs, the technology node plays a role in achieving a high area density, but does only marginally affect energy efficiency. On the other hand, the performance of DIMC is highly dependent

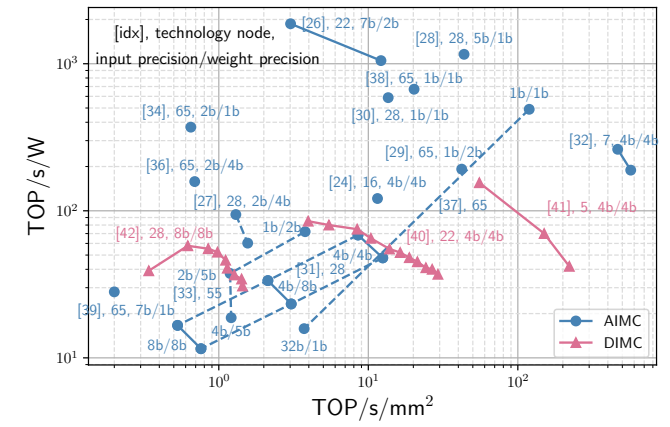


Fig. 4. Benchmarking on AIMC/DIMC architectures. Each point reports the technology node deployed for the design and the input/weight bit precision used.

on the technology node and operand precision: smaller technology nodes guarantee higher computational densities with equal precision and improved power consumption (as in [41] and [42]), while higher precisions cause drops in computational density with similar technology (as in [40] and [41]).

The interplay between technology node, precision, hardware architecture and operating point determines the final efficiencies. It is however hard to discern these relationships based on peak TOPs/W, TOP/s/mm² values alone. To assess the impact of each design parameter, a more in depth modeling effort is required. For this, a unified cost model for DIMC and AIMC is presented in the following section.

IV. ANALYTICAL MODELING FOR IMC

A. A unified energy model for IMC

To enable a fair high-level comparison between AIMC and DIMC, a unified cost model should include the energy contributions of the most dominant components for AIMC

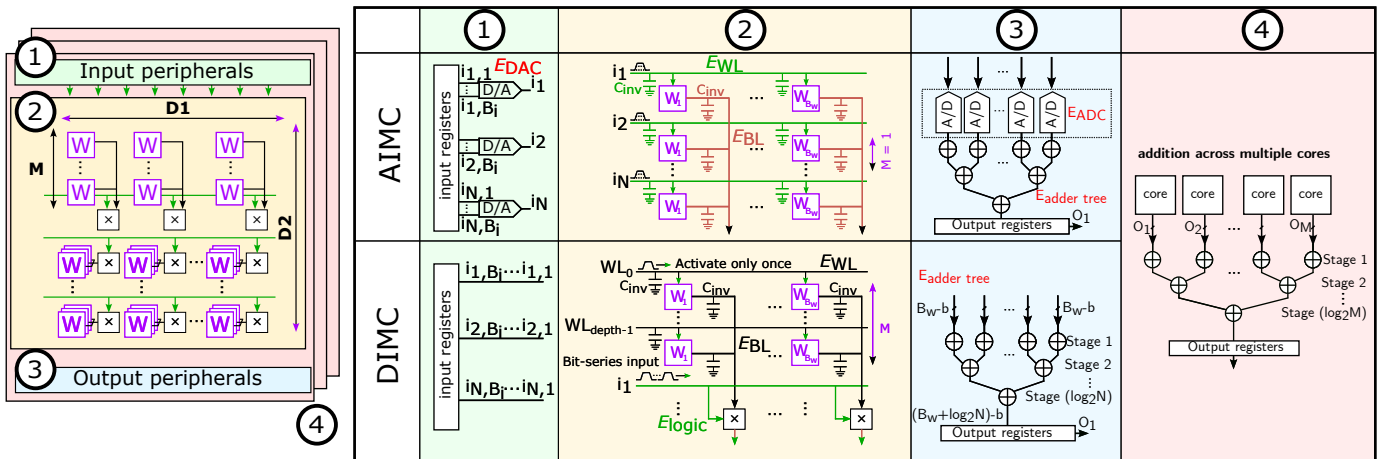


Fig. 3. Modeling template for AIMC and DIMC architectures

Hardware model parameters

R, C	IMC array row, columns resp.
ADC_{res}, DAC_{res}	Bit resolution of the ADC, DAC resp.
WL, BL	SRAM Wordline, Bitline resp.
G_{MUL}, G_{FA}	Number of gates per 1-b multiplier, full adder resp.
M	Number of memory rows multiplexed per vector MAC
B_w	Weight bits stored in parallel in the IMC

Derived parameters

D₁	Activation propagation axis size of the IMC array
D₂	Accumulation axis size of the IMC array
N, B	Adder tree number of inputs, input precision resp.
F	Total number of 1-b full-adders
C_{gate}	Capacitance per gate

Mapping dependent extracted parameters

CC_{prech}	Precharging cycles on the bitlines
CC_{acc}	Cycles of digital accumulation across the adder tree
CC_{BS}	Number of complete DAC conversions required

Technology dependent fitted model parameters

C_{inv}	Capacitance of an inverter, gate resp.
k₁, k₂	ADC model constants from [5]
k₃	DAC energy per conversion step constant

TABLE I
ACRONYM TABLE

and DIMC. Our model is illustrated in Fig. 3. It aims at modeling the datapath components of A/DIMC, while reading and writing from higher-level memories for inputs and outputs access will later be accounted for through integration of the model into the ZigZag DSE framework. The total datapath energy E_{total} can hence be computed as:

$$E_{\text{total}} = E_{\text{MUL}} + E_{\text{ACC}} + E_{\text{peripherals}} \quad (1)$$

where the total energy E_{total} is computed as the sum of the multiplication energy done in the IMC array (E_{MUL}), the energy cost of digital accumulation outside the IMC array (E_{ACC}) and the contribution of peripherals required to access the array and provide the data ($E_{\text{peripherals}}$). All acronyms for symbols in our model are listed in Table I.

B. Multiplication cost

In IMC, the multiplications of the MVM operation occurs within the memory array. The values of the input vector are propagated along wordlines and combined with the data stored in the memory cells (Fig. 3.2). The energy required to execute this operation E_{MUL} can be expressed in the unified model as a sum of two components (Fig. 3.2): the energy related to the charge/discharge of internal capacitances related to the memory cell operations (E_{cell}) and the energy associated with the extra digital logic required to carry out the multiplication (E_{logic}). The latter is only accounted for in DIMC designs, as in AIMC, the multiplication operation takes place in the operation of the memory cell itself.

$$E_{\text{MUL}} = E_{\text{cell}} + E_{\text{logic}} \quad (2)$$

1) E_{cell} contribution: E_{cell} stems from charging and discharging the capacitances across the SRAM wordline (WL) and bitline (BL) associated with a read operation. For AIMC,

the values on the bitlines change every computation cycle since a different input vector is combined with the weights in the array each time. This is not always the case for DIMC: with bit-parallel/bit-serial (BPBS) computations in DIMC ([40]–[42]) the weight values are kept stationary, while different input bits are serially combined across separate cycles. To model this, Eq. 3 scales wth the charging cycles CC_{prech} , being the number of cycles in which the values on the bitlines of the IMC array are non-stationary.

$$E_{\text{cell}} = (E_{\text{WL}} + E_{\text{BL}}) \times CC_{\text{prech}} \quad (3)$$

The WL energy E_{WL} is further computed as in Eq. 4, proportional to the wordline capacitance per cell C_{WL} – assumed to be similar to the capacitance of an inverter in the same technology ($\sim C_{\text{inv}}$) –, the number of weight bits per operand B_w and D_1 , which is the number of operands per memory row.

$$E_{\text{WL}} = C_{\text{WL}} V^2 B_w \times D_1 \quad (4)$$

Similarly, the BL energy E_{BL} is estimated as in Eq. 5, with D_2 being the accumulation dimension of the IMC array and M the row multiplexing factor.

The parameter M identifies the number of rows multiplexed per vector multiplication: in AIMC designs this values is equal to 1, since each row does a vector multiplication in each cycle; for DIMC and near-memory compute (NMC) designs not all rows are activated at once per multiplication, as in [41]

$$E_{\text{BL}} = C_{\text{BL}} V^2 B_w \times D_2 \times M \quad (5)$$

2) E_{logic} contribution: In DIMC designs, the bit-parallel/bit-serial (BPBS) operation is performed, where input bits are serially multiplied with parallel weight bits in the array. The multiplier is typically a single NAND/NOR gate per cell. We therefore use a unified model for the logic cost:

$$E_{\text{logic}} = V^2 C_{\text{gate}} G_{\text{MUL}} \times \text{total MACs} \quad (6)$$

with C_{gate} being the capacitance for standard logic gate ($\approx 2 \times C_{\text{inv}}$). G_{MUL} is the total number of gates per multiplier; in the case of a bit-serial input it equals to the numbers of gates of a 1-b multiplier ($\simeq 1$) times the weight precision B_w .

C. Accumulation cost

Accumulation in the analog domain occurs as a results of charge sharing/injection on each bitline across the memory cells connected to it, which in turn results in a charge and voltage variation over the line (Fig. 2). This contribution is already captured in Eq. 5. The analog value then has to be converted by ADC in the digital domain (E_{ADC}) and eventually combined with other partial results with a digital adder ($E_{\text{adder tree}}$). Digital IMC avoids the need for an ADC, substituted by accumulation in the digital domain (Fig. 3.3). These contributions are accounted for in Eq. 7.

$$E_{\text{ACC}} = E_{\text{ADC}} + E_{\text{adder tree}} \quad (7)$$

1) *ADC energy*: E_{ADC} is estimated using the ADC energy model from [5]

$$E_{\text{ADC}} = (k_1 \times \text{ADC}_{\text{res}} + k_2 4^{\text{ADC}_{\text{res}}}) V^2 \times B_w \times (\text{total MACs} / D_2) \quad (8)$$

with $k_1 = 100 \text{ fJ}$ and $k_2 = 1 \text{ aJ}$. The model assumes one ADC conversion per bitline; this is true for most designs, except for [32], where a 4-bit Flash ADC is used every 4 BLs.

2) *Adder tree energy*: The digital accumulation energy $E_{\text{adder tree}}$ is modeled as:

$$E_{\text{adder tree}} = C_{\text{gate}} G_{\text{FA}} V^2 \times D_1 \times F \times \text{CC}_{\text{acc}} \quad (9)$$

where C_{gate} the gate capacitance for a standard logic gate, G_{FA} the number of gates of a 1-b full adder (FA), assumed to be 5. Assuming a ripple carry-adder, the total number of 1-b full adders F executed per cycle per output channel can be derived as:

$$F = \sum_n^{\log_2 N} (B + n - 1) \frac{N}{2^n} \quad (10)$$

$$= BN + N - B + \log_2 N - 1$$

where N is the number of inputs of the first stage of the tree and B the input precision of the adder operands. Since digital accumulation occurs across core rows for DIMC, N is equal to D_2 for DIMC, while $N = B_w$ for AIMC since accumulation occurs across adjacent bitlines if weight bits are parallelized. B is equal to B_w for DIMC, while for AIMC it is ADC_{res} .

D. Peripherals cost

While for DIMC designs, the drivers propagating the activation values across the wordlines have negligible overhead besides the one already accounted for WL capacitance, multi-bit AIMC accelerators necessitate D/A converters to carry out the task. To this purpose, $E_{\text{peripherals}}$ covers the DAC conversion energy contribution and can be expressed as E_{DAC} (Fig. 3.1)

$$E_{\text{DAC}} = k_3 \text{DAC}_{\text{res}} V^2 \times \text{CC}_{\text{BS}} \quad (11)$$

with $k_3 \sim 44 \text{ fJ}$ and CC_{BS} total number of cycles required for activation bits to be converted to the analog domain.

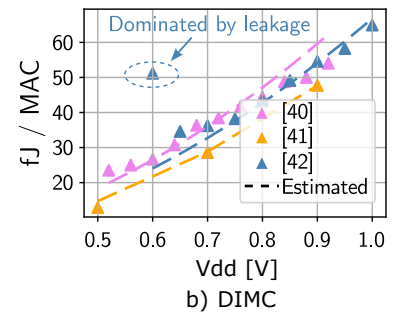
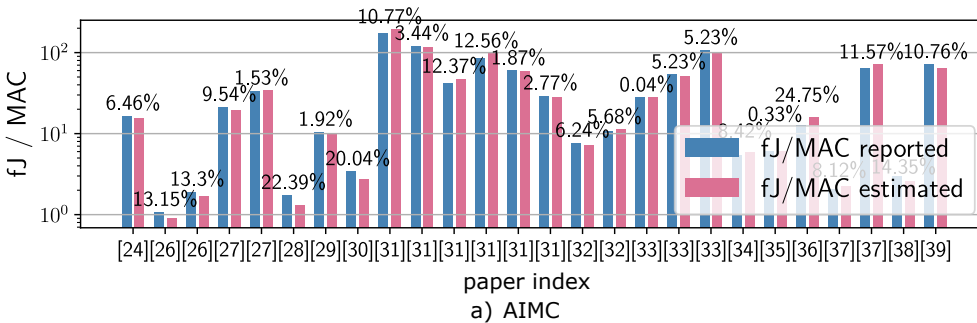


Fig. 5. IMC model validation

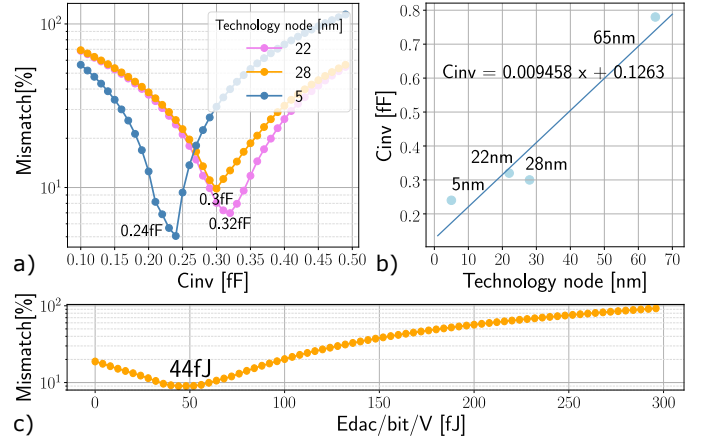


Fig. 6. Technology dependent parameters extraction

E. Technology dependent parameters extraction

The implementation technology impacts the different gate, WL, BL capacitance values of the unified model. To further unify the modeling, all capacitance values are related to a reference capacitance C_{inv} . The C_{inv} values for our model across technologies is linearly regressed across fitted C_{inv} values of the different published DIMC designs ([40]–[42] and [44]) (Fig. 6.a and 6.b). A mismatch between the model and the reported data of $\sim 10\%$ is observed, stemming from 1) modules not taken into account in the model and 2) leakage power, especially under a low voltage and frequency.

The same interpolation principle applies to DAC modeling, to derive a DAC fJ/conversion ($E_{\text{DAC/bit}}$) parameter. As shown in Fig. 6.c, by setting $E_{\text{dac/bit}}$ to $k_3 = 44 \text{ fJ}$, we achieve an average modeling mismatch of $\sim 9\%$ across all AIMC data points used for modeling.

V. VALIDATION

The model has been validated against all design points presented in Sec. III. For AIMC (Fig. 5.a) mismatches between the model and the reported values are within 15% for most designs. Large mismatches are often due to unaccounted overheads or inefficient designs: in [28], [29], [36] reported ADC energies are larger ($\sim 4\times$ than the ones estimated by the model). Other notable mismatches arise when large digital

overheads are present in the macros, such as in [30], [36]. For DIMC (Fig. 5.b) the model matches closely with the reported values, assuming 50% sparsity on the operands; the analytical model however does not cover the leakage contribution, which becomes dominant at low voltages and low frequencies: this can be observed for [42] where measured values at 0.6V steeply diverge from the estimations.

VI. CASE STUDIES

Peak performances reported in literature and Sec. III are not representative for comparing different designs. Instead, architectures should be compared on real workloads to prove their effectiveness. Targeting edge applications, we will compare selected IMC designs on the tinyMLPerf models [22] to assess how AIMC and DIMC array sizes affect mapping efficiency. For this first study, we select from the modeled and validated designs, four designs in the same technology node and with the same operand precision. A summary of the features of the selected designs is reported in Table II. While the macro array size is the same as the one reported on the papers, the number of macros is scaled to make all designs have the same total number of SRAM cells (the size of the largest design) for a fair comparison.

The model with the parameters for the four specific designs has been integrated into the DSE framework ZigZag, allowing the tool to find the optimal spatial and temporal mapping for each architecture and each network layer. The result of the evaluations in terms of energy consumption at macro level and data transfer to/from the macro(s) are shown in Fig. VI.

IMC architectures with large arrays are inherently best suited for networks which consist of layers that have high number of filter kernels and that require large accumulation over input channels and filter dimensions. These layers are usually convolutional ones, with filters larger than 1×1 , or fully connected ones. Those networks that exhibit such characteristics are the DeepAutoEncoder and the Resnet8. It can be seen in the energy breakdown in Fig. VI that AIMC architectures which feature large arrays are performing better than other designs; it has to be noted the benefits vanish if there is no reuse of the operands across computation cycles and weights have to be often rewritten. This occurs for the DeepAutoEncoder network: consisting of only fully connected layers (Fig. 1 operator breakdown), no weight reuse can be obtained across computing cycles and weight data transfers increase energy consumptions. For ResNet8 nonetheless high efficiencies can be achieved, since temporally looping across feature map pixels amortizes the cost of writing the weights. On the other hand, smaller IMC arrays achieve high array utilizations but suffer from large overheads from the array peripherals.

On the opposite scenario, DS-CNN and MobilenetV1 networks are characterized by pointwise (i.e. convolutional layers with 1×1 filters) and depthwise layers: the former require lower accumulation of partial results along the rows and the latter offer no reuse possibility for the activations across output channels mapped on the columns. This makes them

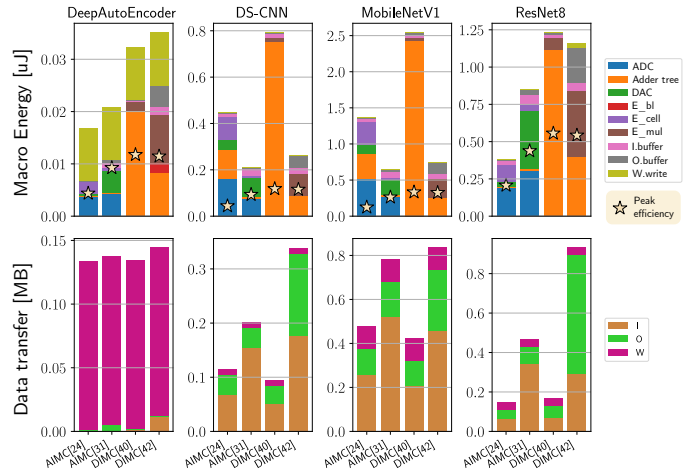


Fig. 7. Energy breakdown at macro level and required data traffic towards outer memory levels for selected IMC designs. Peak energy efficiencies highlight which designs more efficiently map the target workloads

Design	R	C	Macros	Tech [nm]	V	A/W bits
AIMC [24]	1152	256	1	28	0.8	4b/4b
AIMC [31]	64	32	8	28	0.8	4b/4b
DIMC [40]	256	256	4	22	0.8	4b/4b
DIMC [42]	48	4	192	28	0.8	4b/4b

TABLE II

DESIGN CHARACTERISTICS OF THE COMPARED ARCHITECTURES

unsuitable for IMC designs with large arrays as they cause heavy underutilization of the computational resources. For this, those architectures that feature smaller arrays but large number of macros perform better than their counterparts. Increasing the number of macros is a benefit as it allows spatial parallelization of different layer dimensions (O_X, O_Y, G) beside the ones allowed in IMC (namely C, K, F_X, F_Y as shown in Sec. II). However, efficiency benefits at macro level come at a cost: input feature map pixels and partial accumulation values have to be fetched and stored from memory more often since less accumulation is carried out at macro level, as shown in the data transfer breakdown. Future works of design space exploration will focus on mitigating the feature map access overheads by placing extra levels of caching close to the computational macro in such cases, to further evaluate evaluate costs and area trade-offs.

VII. CONCLUSIONS

In this paper, we proposed a unified analytical cost model for AIMC and DIMC to be able to fairly compare across designs with different architectural parameters and technologies. We extract the parameters from a collection of published AIMC and DIMC designs across different technologies and realize a relative mismatch of about 15%. Furthermore, integration of the developed model into the DSE framework ZigZag, allows to not only assess peak performances, but also actual workload performance when mapping real tinyMLperf benchmarks across diverse hardware IMC architectures. Future

work will further deploy this model to assess the relative strengths and potential of AIMC and DIMC.

ACKNOWLEDGMENTS

This work has been supported by KU Leuven and received funding from the Flemish Government (Flanders AI Research Program) and the EU project CONVOLVE.

REFERENCES

- [1] Z. Zhou, X. Chen, E. Li, L. Zeng, K. Luo, and J. Zhang, "Edge intelligence: Paving the last mile of artificial intelligence with edge computing," *Proceedings of the IEEE*, vol. 107, no. 8, pp. 1738–1762, Aug 2019.
- [2] H. Valavi, P. J. Ramadge, E. Nestler, and N. Verma, "A 64-tile 2.4-mb in-memory-computing cnn accelerator employing charge-domain compute," *IEEE Journal of Solid-State Circuits*, vol. 54, no. 6, pp. 1789–1799, June 2019.
- [3] V. Sze, Y.-H. Chen, T.-J. Yang, and J. S. Emer, "Efficient processing of deep neural networks: A tutorial and survey," *Proceedings of the IEEE*, vol. 105, no. 12, pp. 2295–2329, Dec 2017.
- [4] L. Mei, P. Houshmand, V. Jain, S. Giraldo, and M. Verhelst, "Zigzag: Enlarging joint architecture-mapping design space exploration for dnn accelerators," *IEEE Transactions on Computers*, vol. 70, no. 8, pp. 1160–1174, Aug 2021.
- [5] B. Murmann, "Mixed-signal computing for deep neural network inference," *IEEE Transactions on Very Large Scale Integration (VLSI) Systems*, vol. 29, no. 1, pp. 3–13, 2021.
- [6] N. R. Shanbhag and S. K. Roy, "Comprehending in-memory computing trends via proper benchmarking," in *2022 IEEE Custom Integrated Circuits Conference (CICC)*, 2022, pp. 01–07.
- [7] R. Sehgal and J. P. Kulkarni, "Trends in analog and digital intensive compute-in-sram designs," in *2021 IEEE 3rd International Conference on Artificial Intelligence Circuits and Systems (AICAS)*, 2021, pp. 1–4.
- [8] G. W. Burr, S. Lim, B. Murmann, R. Venkatesan, and M. Verhelst, "Fair and comprehensive benchmarking of machine learning processing chips," *IEEE Design & Test*, vol. 39, no. 3, pp. 18–27, 2022.
- [9] S. Rai, M. Liu, A. Gebregiorgis, D. Bhattacharjee, K. Chakrabarty, S. Hamdioui, A. Chattopadhyay, J. Trommer, and A. Kumar, "Perspectives on emerging computation-in-memory paradigms," in *2021 Design, Automation & Test in Europe Conference I& Exhibition (DATE)*, 2021, pp. 1925–1934.
- [10] B. Taylor, Q. Zheng, Z. Li, S. Li, and Y. Chen, "Processing-in-memory technology for machine learning: From basic to ASIC," *IEEE Transactions on Circuits and Systems II: Express Briefs*, vol. 69, no. 6, pp. 2598–2603, 2022.
- [11] S. Yu, H. Jiang, S. Huang, X. Peng, and A. Lu, "Compute-in-memory chips for deep learning: Recent trends and prospects," *IEEE Circuits and Systems Magazine*, vol. 21, no. 3, pp. 31–56, 2021.
- [12] M. Ali, S. Roy, U. Saxena, T. Sharma, A. Raghunathan, and K. Roy, "Compute-in-memory technologies and architectures for deep learning workloads," *IEEE Transactions on Very Large Scale Integration (VLSI) Systems*, vol. 30, no. 11, pp. 1615–1630, 2022.
- [13] S. K. Gonugondla, C. Sakr, H. Dbouk, and N. R. Shanbhag, "Fundamental limits on the precision of in-memory architectures," in *2020 IEEE/ACM International Conference On Computer Aided Design (ICCAD)*, 2020, pp. 1–9.
- [14] —, "Fundamental Limits on Energy-Delay-Accuracy of In-memory Architectures in Inference Applications," *CoRR*, vol. abs/2012.13645, 2020, arXiv: 2012.13645. [Online]. Available: <https://arxiv.org/abs/2012.13645>
- [15] M. Kang, Y. Kim, A. D. Patil, and N. R. Shanbhag, "Deep in-memory architectures for machine learning—accuracy versus efficiency trade-offs," *IEEE Transactions on Circuits and Systems I: Regular Papers*, vol. 67, no. 5, pp. 1627–1639, 2020.
- [16] D. Bhattacharjee, N. Laubeuf, S. Cosemans, I. Papistas, A. Maliik, P. Debacker, M. H. Na, and D. Verkest, "Design-technology space exploration for energy efficient aimc-based inference acceleration," in *2021 IEEE International Symposium on Circuits and Systems (ISCAS)*, 2021, pp. 1–5.
- [17] S. Spetalnick and A. Raychowdhury, "A practical design-space analysis of compute-in-memory with sram," *IEEE Transactions on Circuits and Systems I: Regular Papers*, vol. 69, no. 4, pp. 1466–1479, 2022.
- [18] C.-J. Jhang, C.-X. Xue, J.-M. Hung, F.-C. Chang, and M.-F. Chang, "Challenges and trends of sram-based computing-in-memory for ai edge devices," *IEEE Transactions on Circuits and Systems I: Regular Papers*, vol. 68, no. 5, pp. 1773–1786, 2021.
- [19] U. Saxena, I. Chakraborty, and K. Roy, "Towards adc-less compute-in-memory accelerators for energy efficient deep learning," in *2022 Design, Automation I& Test in Europe Conference I& Exhibition (DATE)*, 2022, pp. 624–627.
- [20] S. Yang, D. Bhattacharjee, V. B. Y. Kumar, S. Chatterjee, S. De, P. Debacker, D. Verkest, A. Mallik, and F. Cathoor, "Aero: Design space exploration framework for resource-constrained cnn mapping on tile-based accelerators," *IEEE Journal on Emerging and Selected Topics in Circuits and Systems*, vol. 12, no. 2, pp. 508–521, 2022.
- [21] X. Peng, R. Liu, and S. Yu, "Optimizing weight mapping and data flow for convolutional neural networks on rram based processing-in-memory architecture," in *2019 IEEE International Symposium on Circuits and Systems (ISCAS)*, 2019, pp. 1–5.
- [22] C. Banbury, V. J. Reddi, P. Torelli, J. Holleman, N. Jeffries, C. Kiraly, P. Montino, D. Kanter, S. Ahmed, D. Pau *et al.*, "Mlperf tiny benchmark," *Proceedings of the Neural Information Processing Systems Track on Datasets and Benchmarks*, 2021.
- [23] A. Gholami, S. Kim, Z. Dong, Z. Yao, M. W. Mahoney, and K. Keutzer, "A survey of quantization methods for efficient neural network inference," *CoRR*, vol. abs/2103.13630, 2021. [Online]. Available: <https://arxiv.org/abs/2103.13630>
- [24] H. Jia, M. Ozatay, Y. Tang, H. Valavi, R. Pathak, J. Lee, and N. Verma, "15.1 a programmable neural-network inference accelerator based on scalable in-memory computing," in *2021 IEEE International Solid-State Circuits Conference (ISSCC)*, vol. 64, 2021, pp. 236–238.
- [25] P. Houshmand, S. Cosemans, L. Mei, I. Papistas, D. Bhattacharjee, P. Debacker, A. Mallik, D. Verkest, and M. Verhelst, "Opportunities and limitations of emerging analog in-memory compute dnn architectures," in *2020 IEEE International Electron Devices Meeting (IEDM)*, 2020, pp. 29.1.1–29.1.4.
- [26] I. A. Papistas, S. Cosemans, B. Rooseleer, J. Doevevspeck, M.-H. Na, A. Mallik, P. Debacker, and D. Verkest, "A 22 nm, 1540 top/s/w, 12.1 top/s/mm2 in-memory analog matrix-vector-multiplier for dnn acceleration," in *2021 IEEE Custom Integrated Circuits Conference (CICC)*, 2021, pp. 1–2.
- [27] J.-W. Su, Y.-C. Chou, R. Liu, T.-W. Liu, P.-J. Lu, P.-C. Wu, Y.-L. Chung, L.-Y. Hung, J.-S. Ren, T. Pan, S.-H. Li, S.-C. Chang, S.-S. Sheu, W.-C. Lo, C.-I. Wu, X. Si, C.-C. Lo, R.-S. Liu, C.-C. Hsieh, K.-T. Tang, and M.-F. Chang, "16.3 a 28nm 384kb 6t-sram computation-in-memory macro with 8b precision for ai edge chips," in *2021 IEEE International Solid-State Circuits Conference (ISSCC)*, vol. 64, 2021, pp. 250–252.
- [28] J. Lee, H. Valavi, Y. Tang, and N. Verma, "Fully row/column-parallel in-memory computing sram macro employing capacitor-based mixed-signal computation with 5-b inputs," in *2021 Symposium on VLSI Circuits*, 2021, pp. 1–2.
- [29] H. Jia, H. Valavi, Y. Tang, J. Zhang, and N. Verma, "A programmable heterogeneous microprocessor based on bit-scalable in-memory computing," *IEEE Journal of Solid-State Circuits*, vol. 55, no. 9, pp. 2609–2621, 2020.
- [30] S. Yin, B. Zhang, M. Kim, J. Saikia, S. Kwon, S. Myung, H. Kim, S. Joon Kim, M. Seok, and J.-s. Seo, "Pimca: A 3.4-mb programmable in-memory computing accelerator in 28nm for on-chip dnn inference," in *2021 Symposium on VLSI Circuits*, 2021, pp. 1–2.
- [31] X. Si, Y.-N. Tu, W.-H. Huang, J.-W. Su, P.-J. Lu, J.-H. Wang, T.-W. Liu, S.-Y. Wu, R. Liu, Y.-C. Chou, Z. Zhang, S.-H. Sie, W.-C. Wei, Y.-C. Lo, T.-H. Wen, T.-H. Hsu, Y.-K. Chen, W. Shih, C.-C. Lo, R.-S. Liu, C.-C. Hsieh, K.-T. Tang, N.-C. Lien, W.-C. Shih, Y. He, Q. Li, and M.-F. Chang, "15.5 a 28nm 64kb 6t sram computing-in-memory macro with 8b mac operation for ai edge chips," in *2020 IEEE International Solid-State Circuits Conference - (ISSCC)*, 2020, pp. 246–248.
- [32] Q. Dong, M. E. Sinangil, B. Erbagci, D. Sun, W.-S. Khwa, H.-J. Liao, Y. Wang, and J. Chang, "15.3 a 351tops/w and 372.4gops compute-in-memory sram macro in 7nm finfet cmos for machine-learning applications," in *2020 IEEE International Solid-State Circuits Conference - (ISSCC)*, 2020, pp. 242–244.
- [33] X. Si, J.-J. Chen, Y.-N. Tu, W.-H. Huang, J.-H. Wang, Y.-C. Chiu, W.-C. Wei, S.-Y. Wu, X. Sun, R. Liu, S. Yu, R.-S. Liu, C.-C. Hsieh, K.-T. Tang, Q. Li, and M.-F. Chang, "24.5 a twin-8t sram computation-in-memory macro for multiple-bit cnn-based machine learning," in *2019*

IEEE International Solid- State Circuits Conference - (ISSCC), 2019, pp. 396–398.

- [34] J. Yue, X. Feng, Y. He, Y. Huang, Y. Wang, Z. Yuan, M. Zhan, J. Liu, J.-W. Su, Y.-L. Chung, P.-C. Wu, L.-Y. Hung, M.-F. Chang, N. Sun, X. Li, H. Yang, and Y. Liu, “15.2 a 2.75-to-75.9tops/w computing-in-memory nn processor supporting set-associate block-wise zero skipping and ping-pong cim with simultaneous computation and weight updating,” in *2021 IEEE International Solid- State Circuits Conference (ISSCC)*, vol. 64, 2021, pp. 238–240.
- [35] R. A. Rasul and M. S.-W. Chen, “A 128x128 sram macro with embedded matrix-vector multiplication exploiting passive gain via mos capacitor for machine learning application,” in *2021 IEEE Custom Integrated Circuits Conference (CICC)*, 2021, pp. 1–2.
- [36] J. Yue, Z. Yuan, X. Feng, Y. He, Z. Zhang, X. Si, R. Liu, M.-F. Chang, X. Li, H. Yang, and Y. Liu, “14.3 a 65nm computing-in-memory-based cnn processor with 2.9-to-35.8tops/w system energy efficiency using dynamic-sparsity performance-scaling architecture and energy-efficient inter/intra-macro data reuse,” in *2020 IEEE International Solid- State Circuits Conference - (ISSCC)*, 2020, pp. 234–236.
- [37] C. Yu, T. Yoo, T. T.-H. Kim, K. C. Tshun Chuan, and B. Kim, “A 16k current-based 8t sram compute-in-memory macro with decoupled read/write and 1-5bit column adc,” in *2020 IEEE Custom Integrated Circuits Conference (CICC)*, 2020, pp. 1–4.
- [38] Z. Jiang, S. Yin, J.-S. Seo, and M. Seok, “C3sram: An in-memory-computing sram macro based on robust capacitive coupling computing mechanism,” *IEEE Journal of Solid-State Circuits*, vol. 55, no. 7, pp. 1888–1897, 2020.
- [39] A. Biswas and A. P. Chandrakasan, “Conv-ram: An energy-efficient sram with embedded convolution computation for low-power cnn-based machine learning applications,” in *2018 IEEE International Solid - State Circuits Conference - (ISSCC)*, 2018, pp. 488–490.
- [40] Y.-D. Chih, P.-H. Lee, H. Fujiwara, Y.-C. Shih, C.-F. Lee, R. Naous, Y.-L. Chen, C.-P. Lo, C.-H. Lu, H. Mori, W.-C. Zhao, D. Sun, M. E. Sinangil, Y.-H. Chen, T.-L. Chou, K. Akarvardar, H.-J. Liao, Y. Wang, M.-F. Chang, and T.-Y. J. Chang, “16.4 an 89tops/w and 16.3tops/mm² all-digital sram-based full-precision compute-in memory macro in 22nm for machine-learning edge applications,” in *2021 IEEE International Solid- State Circuits Conference (ISSCC)*, vol. 64, 2021, pp. 252–254.
- [41] H. Fujiwara, H. Mori, W.-C. Zhao, M.-C. Chuang, R. Naous, C.-K. Chuang, T. Hashizume, D. Sun, C.-F. Lee, K. Akarvardar, S. Adham, T.-L. Chou, M. E. Sinangil, Y. Wang, Y.-D. Chih, Y.-H. Chen, H.-J. Liao, and T.-Y. J. Chang, “A 5-nm 254-tops/w 221-tops/mm² fully-digital computing-in-memory macro supporting wide-range dynamic-voltage-frequency scaling and simultaneous mac and write operations,” in *2022 IEEE International Solid- State Circuits Conference (ISSCC)*, vol. 65, 2022, pp. 1–3.
- [42] F. Tu, Y. Wang, Z. Wu, L. Liang, Y. Ding, B. Kim, L. Liu, S. Wei, Y. Xie, and S. Yin, “A 28nm 29.2tflops/w bf16 and 36.5tops/w int8 reconfigurable digital cim processor with unified fp/int pipeline and bitwise in-memory booth multiplication for cloud deep learning acceleration,” in *2022 IEEE International Solid- State Circuits Conference (ISSCC)*, vol. 65, 2022, pp. 1–3.
- [43] J.-s. Seo, J. Saikia, J. Meng, W. He, H.-s. Suh, Anupreetham, Y. Liao, A. Hasssan, and I. Yeo, “Digital versus analog artificial intelligence accelerators: Advances, trends, and emerging designs,” *IEEE Solid-State Circuits Magazine*, vol. 14, no. 3, pp. 65–79, 2022.
- [44] N. Shah, L. I. G. Olascoaga, W. Meert, and M. Verhelst, “Problp: A framework for low-precision probabilistic inference,” in *Proceedings of the 56th Annual Design Automation Conference 2019*, ser. DAC '19. New York, NY, USA: Association for Computing Machinery, 2019. [Online]. Available: <https://doi.org/10.1145/3316781.3317885>